Combining constitutive materials modeling with atomic force microscopy to understand the mechanical properties of living cells

Mike McElfresh*†, Eveline Baesu*‡, Rod Balhorn*, James Belak*, Michael J. Allen§, and Robert E. Rudd*

*Lawrence Livermore National Laboratory, Livermore, CA 94550; ‡Department of Engineering Mechanics, University of Nebraska, Lincoln, NE 68588; and §Biometrology, Incorporated, 851 West Midway Avenue, Alameda, CA 94501

Edited by Calvin F. Quate, Stanford University, Stanford, CA, and approved February 21, 2002 (received for review October 1, 2001)

The goal of this work is to study the properties of living cells and cell membranes by using atomic force microscopy. During atomic force microscopy (AFM) measurement, there is a strong mechanical coupling between the AFM tip and the cell. The purpose of this paper is to present a model of the overall mechanical response of the cell that allows us to separate out the mechanical response of the cell from the local surface interactions we wish to quantify. These local interactions include recognition (or binding) events between molecules bound to an AFM tip (e.g., an antibody) and molecules or receptors on the cell surface (e.g., the respective antigen). The computational model differs from traditional Hertzian contact models by explicitly taking into account the mechanics of the biomembrane and cytoskeleton. The model also accounts for the mechanical response of the living cell during arbitrary deformation. The indentation of a bovine sperm cell is used to test the validity of this model, and further experiments are proposed to fully parameterize the model.

The surface of the living cell is a highly complex heterogeneous structure containing a variety of lipid, protein, and carbohydrate components. The organization of the cell's exterior ''sensing elements'' and other specialized regions of the membrane is tailored to reflect the function of the cell and serves vital roles in cell–cell interactions, cell signaling, and cell–surface interactions. The changes that occur in these important chemical/mechanical phenotypes during the development of cancer and other diseases may be understood in much more detail, thereby allowing the relationships between specific phenotypes to cell and tissue normo- and pathophysiology, prognosis, and therapy to be discerned (1). Recent studies have shown that the components that comprise the membrane are segregated into domains that are dynamic and change in response to external and internal stimuli (2–5). This segregation appears to be controlled by a variety of factors, including the composition of the lipids, interactions with the cytoskeleton or extracellular matrix, and physical or structural barriers to diffusion (6–9). Although these barriers usually limit the random movement of receptors used in signaling and recognition and maintain them in a particular environment, proteins and carbohydrates are often relocalized and recruited into a particular region of the cell surface to facilitate cell function. In some cases, such as the sperm cell, dramatic changes in the composition of the membrane and the location and distribution of its proteins (receptors) occur throughout its development. In other cases, more subtle changes often occur later in the life of the cell and lead to cancer or other diseases, such as multiple sclerosis.

Atomic force microscopy (AFM) has developed rapidly during the past decade, providing nanometer-scale resolution in the imaging of biological materials ranging in size from single molecules to intact cells. Although the best data have been obtained from studies of macromolecules (proteins, nucleic acids, and their complexes), AFM images of mouse and bull sperm have been obtained that rival the resolution of electron microscopy (EM) (10, 11). Unlike EM, however, AFM imaging can be performed in fluid on living cells.

More recent developments in AFM now allow the detection of molecular recognition events between single molecules using ligands attached to AFM tips for the recognition of receptors bound on rigid surfaces (12–25). By monitoring the cantilever deflection during approach–retraction cycles (i.e., force–volume/force–distance curves) at a constant (lateral) position on the sample, unbinding forces (i.e., the maximum force at the moment of receptor–ligand detachment) have been determined for various ligand–receptor pairs, including biotin–avidin (13, 14, 21), DNA bases (15), antibody–antigen (16–22), and cell-recognition proteins (23). This development has made it possible to use a single receptor molecule bound to the tip of an AFM cantilever to map the locations of ligands bound on solid surfaces (26). The goal of our project is to enable this ''recognition mapping'' method to be used in the study of the surfaces of living cells.

Moving recognition microscopy onto living cell surfaces poses some particular challenges related to the fact that there is a mechanical coupling between the measuring system and the object to be observed. Difficulties arise because of the softness of the cell components, the size of the cell, and the need to work in an aqueous environment. Another view might attribute the difficulties to the size of cells. The net result of each of these challenges is that a rather large deformation of the cell may be necessary to measure its mechanical properties, even at a single receptor site.

An immediate technical challenge then is to separate the interesting local characteristics of the receptor site from the gross deformation of the cell as a whole, requiring at the very least an understanding of how cellular anatomy translates into mechanical response. Here we approach this challenge by developing a computational model of the cell and design a set of experiments to parameterize the model. The framework for the

---

This paper results from the Arthur M. Sackler Colloquium of the National Academy of Sciences, ''Nanoscience: Underlying Physical Concepts and Phenomena,'' held May 18–20, 2001, at the National Academy of Sciences in Washington, DC.

This paper was submitted directly (Track II) to the PNAS office.

Abbreviations: AFM, atomic force microscopy; CSG, coverslip glass; TSB, Tris–saline buffer; F(d), force–distance.

†To whom reprint requests should be addressed at: Materials Research Institute; L-418, Lawrence Livermore National Laboratory, 7000 East Avenue, Livermore, CA 94550. E-mail: mcelfresh1@llnl.gov.

model is borrowed from solid mechanics, which has been developed to describe a broad range of materials, including rubbers and other soft materials.

The modeling techniques we describe here are not based on a Hertzian analysis of the deformation, as has been common practice in AFM literature (27). It has been recognized that the material constants extracted through Hertzian analysis are, in fact, not characteristic constants of the system but rather depend on the way the measurement is made. The problem is that the techniques of AFM and nanoindentation have been developed for relatively hard materials such as metals, semiconductors, and ceramics. These systems typically offer a flat surface for analysis, and they allow only a small indentation before they yield plastically or fracture, which is the kind of system described well by the theory of elastic indentation developed by Hertz (28). The Hertz theory makes a few basic assumptions:

- The material under study comprises a large system with a flat surface (a half-space).
- The material returns to its original shape when the load is released (elasticity).
- The material is linear: doubling the stress doubles the strain (Hooke's Law).
- There is no preferred direction or point in the bulk material (isotropy and homogeneity).

In addition, Hertz's original theory did not allow for adhesion of the indenter to the material, but the theory has been extended by Johnson, Kendall, and Roberts to account for the possibility that the surfaces would stick together (29).

It is clear that the assumptions of the Hertzian theory are not applicable to living cells. The deformation of a cell during a typical experiment is a considerable fraction of the size of a cell, so the half-space assumption is incorrect (finite size is important); the deformation may depend on the rate at which the force is applied (viscoelasticity may be important); large deformations lead to a nonlinear response (hyperelasticity); and the structure within the cell can lead to some regions being harder than others (inhomogeneity and perhaps anisotropy). Here we focus on the problems of finite domain and nonlinear elasticity.

We have selected the bovine sperm cell for these studies. This cell was selected for several features, including the discreteness of the cell and the reproducible well-defined shape. We are primarily interested in the anterior of the cell, and the tail's effect may be safely neglected. The interior of the cell is composed primarily of chromatin (protein-coated DNA) and water and, for the purposes of this discussion, it is modeled as a homogeneous incompressible medium. The chromatin is understood to play an important role in determining the cell shape, but its elastic properties are not expected to influence small-to-moderate deformations of the dorsal region of the cell.

Experiment. Previously frozen bovine sperm cells were plated onto 0.170-mm-thick coverslip glass (CSG) that was pretreated with a coating of 1% poly-L-lysine. The CSG was then transferred to the bottom of a Petri dish containing Tris–saline buffer (TSB) (150 mM NaCl/10 mM Tris, pH 7.2), and freshly suspended cells were added to the perimeter of the Petri dish such that the cells were not introduced directly above the CSG. The cells were incubated in the Petri dish for approximately 15 min or until adequate adsorption of living cells to the CSG had occurred (as monitored with a light microscope). The CSG was then carefully removed from the Petri dish such that a dome of TSB fluid was retained over the adsorbed cells and the backside of the CSG wicked completely dry with a tissue. The CSG was then mounted to the AFM stub by using a small piece of double-sided sticky tape and loaded into the AFM.

The model DNP AFM probe from Digital Instruments (Santa Barbara, CA) was chosen for these measurements. It had been selected because the large radius of curvature of its probe tip and the ultra-low spring constant of its cantilever allowed us to interrogate the living cells to suit our objectives without damage to the cells. Before measurements, the size and shape of AFM probe were characterized by using a titanium reference sample from Digital Instruments/Veeco and the TGG01 silicon grating from MikroMasch (Tallinn, Estonia). This probe's cantilever is made of silicon nitride, is triangular, 200 microns in length, and has a spring constant of 0.06 N/m. Cantilever sensitivity (i.e., cantilever deflection signal vs. voltage applied to move the z-piezo) was first determined by using an extremely hard reference sample made of sapphire. The probe was then used to make force measurements (under TSB) in three predetermined subregions of the bovine sperm cell. The force curves were taken by using a total z-scan size of 600–800 nm with a penetration depth into the cell of about 350 nm. The z-scan rate used was approximately 10 Hz. After the force curve analysis, the probe was again characterized by using the titanium reference.

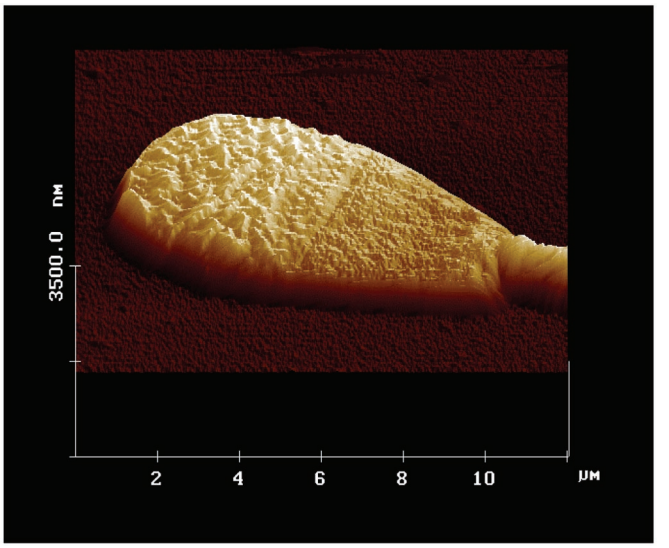

Fig. 1. AFM measurement of topography of the bovine sperm cell.

Fig. 1 shows the topography of a bovine sperm cell analyzed by contact mode AFM under TSB. Several regions of the cell are distinguishable, including the acrosome, midpiece, postacrosomal segments, and flagellum. The three segments are distinguished by the amplitude of the local height variations, with the acrosomal region having variations on the order of 100 nm, the midpiece exhibiting 5-nm variations, and the postacrosomal region 15-nm variations in local height. In addition, a fairly clearly defined 30-nm depression running across the short axis of the cell body identifies the boundary between the midpiece and postacrosomal segments. These amplitude variations are consistent with the numbers of membrane layers present in each region. The total cell thickness at each of the three regions as measured by AFM under TSB is as follows: acrosomal region, 797 nm; midpiece, 689 nm; postacrosomal region, 610 nm. The 100-nm height variations seen in the acrosomal region are because of the presence of the inner and outer acrosomal membranes that encapsulate the anterior end of the cell. The 5-nm height variations measured for the midpiece are because of a flat belt-like structure corresponding to the equatorial segment. The postacrosomal region's 15-nm height variations are because of a delicate highly porous layer corresponding to the perinuclear material. The pores are approximately 80 nm in diameter.

Fig. 2 shows force–distance [$F(d)$] curves for each of the three regions: acrosomal, midpiece, and postacrosomal segments, which are evident in the topographic image. The $F(d)$ curves

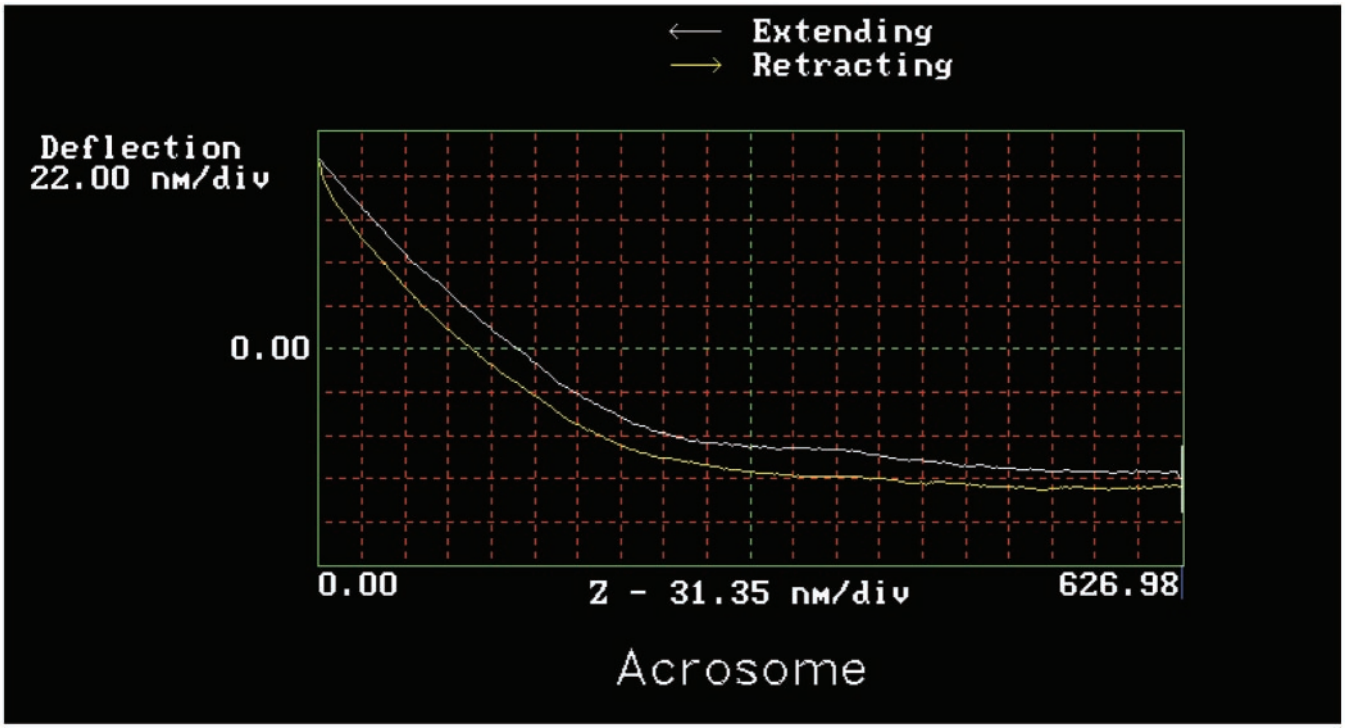

Fig. 2. Force vs. distance curves for the acrosome.

show three regimes: (*i*) essentially flat on initial approach toward the cell surface (i.e., from ≈625 to ≈260 nm), (*ii*) a shallow nearly linear slope for over 100 nm once the tip is engaged with the cell, and (*iii*) the slope increases nonlinearly for the final approach of the tip as the cell is further compressed. These three behaviors correspond, respectively, to (*i*) the tip moving through the fluid with nominal resistance, (*ii*) a stiffness of about 0.03 N/m, and then (*iii*) a continually increasing stiffness. Hysteresis is exhibited; however, because the approach and retraction curves show changes at the same d values, we conclude that the hysteresis is probably associated with irreversible displacements of the media between membrane layers.

Modeling. The goal of the modeling described here is to obtain a mathematical relation between the deformation of the cell and the applied forces. This relation will predict the deformation under a given force or alternatively allow the determination of the applied forces once the deformation (shape) is known. The modeling has two stages: first we model the mechanical properties of a membrane, and then we model the AFM experiment. The membrane is modeled as a nonlinear elastic medium, whereas the AFM experiment is considered to be a point–load problem (a force applied at just one point) on a sector of a sphere.

We assume the response observed in our AFM experiments on living cells is elastic, which means that the cell will return to its original shape once the applied force is removed. There is some evidence of a viscoelastic response under certain conditions that will not be addressed here (27).

Because of the small thickness of the membrane with respect to the size of the cell, a direct two-dimensional continuum model is used to model the combination of membrane and associated cytoskeleton. The third dimension, the thickness of the membrane, is essentially atomistic in nature and is regarded as negligible from the point of view of continuum deformations. Each phospholipid bilayer is ≈5 nm thick, and the composite membrane is roughly 30 nm thick, varying somewhat from site to site on the cell, which is very small in comparison with the cell length of 10,000 nm. Similarly, the tip of the AFM cantilever used in our experiments is approximately 50 nm in radius, which is comparable to the thickness of the membrane and negligible compared with the cell dimensions, justifying the use of a point–load treatment in our model. We return to this point below, showing that the model is internally consistent, because the estimated curvature of the membrane is larger than the radius of the tip, so the point load is a reasonable first approximation. In this model, we neglect the multilayer nature of the membrane.

Modeling the Membrane. The characteristic quantity of our model of the nonlinear elastic fluid membrane is the strain energy/unit mass, w, of the membrane, i.e., the energy required to deform the membrane. Once the strain energy is determined, the stress function can be easily obtained with the methods of elasticity by taking the derivatives of the strain energy with respect to strain and curvature. When the membrane is treated as a two-dimensional (closed) nonlinearly elastic fluid continuum, w must be a scalar function of two quantities, J and H, which characterize the local stretching and bending of the membrane, respectively (30). More precisely, J characterizes the local change in area, and H is the mean curvature. There have been widespread attempts to use classical Kirchhoff linear plate bending theory for solids to model biomembranes and surfactant systems. (see refs. 30–33 and refs. therein). The invariant H used there was the invariant of a tensor characterizing the change in curvature, say $\mathbf{k}$, which is not appropriate for describing fluidity, for reasons discussed in ref. 30. Nevertheless, when the plate model is used to describe small deformations, $\mathbf{k}$ approximates well the curvature tensor used to describe fluids (whose invariant is H) and therefore to this order of approximation, the two theories would yield the same result for small deformations. But the deformation of soft tissue, especially the deformation of a cell membrane in an AFM experiment, would certainly yield very large deformations, for which a form of w appropriate for fluids (that depends on J and H) is used.

The dependence of w on the two quantities mentioned above

is considered in general, in an additive way, through two coefficients T and A, respectively,

$$w = TJ + AH^2 \quad [1]$$

where T is the stretching modulus and A is the bending modulus. The invariant H appears squared in the expression for w to ensure the physical requirement that the membrane's local response is the same for upward as well as downward bending. The bending moduli are materials constants specific to this cell for the membrane. A more detailed discussion of this energy function will be given elsewhere (E.B., R.E.R., M.M., J.B., and R.B., unpublished work; ref. 34). Here we just mention that A can be related to the moments necessary to deform a plane membrane into a cylindrical surface.

Modeling the AFM Experiment. To model the AFM experiment, initially the cell is considered to be a sector of a sphere that is subjected to a point force F, at the pole. The actual shape that the cell takes on under an applied force is given as a solution to a set of partial differential equations (the Euler–Lagrange equations) that are derived on the basis of energy minimization considerations. The axisymmetry in the problem reduces these partial differential equations to ordinary differential equations with eight associated boundary conditions, which can be solved numerically. Considering half the cell as a sector of a sphere is particularly appropriate to the bovine sperm cell, which has a definite shape.

The media outside of the membrane (the liquid droplet surrounding it and the cytoplasm) are assumed to be incompressible, acting on the membrane through a net pressure. This assumption seems to be reasonable because more than 50% of the volume inside the cell is water. By enforcing this constraint, the net pressure through the membrane appears in the equations as a Lagrange multiplier to be calculated after the equations are solved, from the condition of preserved volume. Therefore, it is not necessary to directly measure the pressure. The input parameter to this model is the applied force, and what is sought is the deformation (the profile of the deformed cell), that is, the coordinates of each point of the membrane as functions of the arc length along the meridian of the sphere.

The dependence of w on J can be avoided if we use the assumption that the local area of the membrane is preserved. This constraint yields one relation between the variables in question. In that case, T can be calculated after the fact, as another Lagrange multiplier. Alternatively, we can leave it in the strain energy and actually test the assumption that the area is preserved (see ref. 35). Therefore, change in the strain energy, Δw, is due only to change in H^2.

For a given value of the parameter A, the shape of the cell can be computed by minimizing the strain energy. The optimal value of A gives the closest agreement between the computed and measured shape of the cell. What is required from experiment is information about the deformed surface of the cell. The parameterized strain energy is then used to compute the mechanical properties of the membrane. Further details of this model will be presented elsewhere (E.B., R.E.R., M.M., J.B. and R.B., unpublished work; ref. 34).

Although we currently have no direct measurement of the deformed cell shape, we can estimate the curvature within the context of our model assuming the membrane behaves like a liquid crystal (3). Within this assumption, $A \approx 10^{-12}$ erg (1 erg = 0.1 μJ). From our preliminary force-displacement preliminary plot in Fig. 2, we see that the maximum force $F = 6.6 \times 10^{-9}$ N corresponds to the displacement $d = 60 \times 10^{-9}$ m. The total work done by external forces is $(0.5)Fd \approx 4 \times 10^{-16}$ Nm, which is balanced by the work stored in the membrane, i.e.,

$$Fd = 2\int_{\text{total surface}} \Delta w da = 2\int_{\text{total surface}} A\Delta(H^2)\, da, \quad [2]$$

where da is the area element. The integral can be estimated by using an average value of ΔH^2, say Δh^2, where $h^2 = \int_{\text{total surface}} H^2\, da$. With these numerical values, and using a membrane thickness, $t = 10^{-8}$ m, the quantity $t^2 \times (h^2_{\text{final}} - h^2_{\text{initial}})$ is of the order of 10^{-3}, demonstrating that the length scales in the problem are well within the range of applicability of our two-dimensional continuum model. Further, these estimates give an average radius of curvature of 10^{-6} m for the deformed membrane. The quantity h^2 is approximately equal to $4/R^2$, where R is the average radius of curvature. The radius of curvature at the pole, where the force is applied, gives most of the contribution to this average value. Using Eq. **2** and the experimental force-displacement curve, we estimate the maximum radius of curvature of the membrane to be 10^{-6} m. This value is two orders of magnitude greater than the radius of the tip (10^{-8} m) and the thickness of the membrane (10^{-8} m), justifying the approximation of modeling the AFM–cell interaction as a point load.

Discussion

We have selected a particular strategy for moving recognition microscopy onto a living cell surface. To separate the local characteristics of the receptor sites, which we plan to study with recognition microscopy, from the gross deformation of the cell as a whole, we have developed a computational model to help us understand how cellular anatomy translates into mechanical response. This approach is because mechanical response associated with the softness of the ''materials'' comprising the cell will be convoluted with the mechanical response associated with the recognition events that we want to study.

In the present work, we have measured both a highly detailed topology of the bovine sperm cell and force vs. distance curves. In combination with the computational model, only the net force was used here. By using this net force with a published value of the parameter A, the model was used to derive a prediction for the deformation of the membrane. We are presently developing an experimental method that will allow the direct measurement of the cell deformation under a point load. With a quantitative knowledge of the point load force and the cell deformation profile the strain energy/unit mass, w, of the membrane can be parameterized. With w parameterized, we then know the mechanical response of the cell membrane under any combination of forces.

The combination of model plus experiment envisioned here might be refined in a number of ways to accommodate observed phenomena that have been neglected in this first phase. For example, it is known that there is a force generated in response to the dragging of entities through, or across, the cell membrane. To accommodate this in the theory, one may add terms that depend on the time derivative of the surface metric to the membrane part of the stress and on the derivative of the curvature to the bending part. The coefficients associated with these additional terms are the viscosity associated with strain rate and with flexure rate, respectively. The resulting constitutive equations may then be used in the existing equations of motion for the surface to predict the coupling between deformation and deformation rate generated by nonequilibrium processes associated with cell response. This evolution of the theoretical model can be tested then with suitable experiments that will emphasize its new features.

We thank Stuart Lindsay, David Steigman, Michael Ortiz, and Carl Melius for useful discussions. This work was performed under the auspices of the U.S. Department of Energy by the University of California, Lawrence Livermore National Laboratory (LLNL), under Contract No. W-7405-Eng-48. We gratefully acknowledge funding through the LLNL Laboratory Directed Research and Development Grant 01-ERI-001. E.B. thanks the Department of Applied Science, University of California, Davis, and the LLNL Materials Research Institute for their hospitality during her visit.

1. Lekka, M., Lekki, J., Marszalek, M., Golonka, P., Stachura, Z., Cleff, B. & Hrynkiewicz, A. Z. (1999) *Appl. Surf. Sci.* **141,** 345–349.
2. Primakoff, P. & Myles, D. G. (1983) *Dev. Biol.* **98,** 417–428.
3. Friend, D. S. (1989) *Ann. NY Acad. Sci.* **567,** 208–221.
4. Edidin, M. (1997) *Curr. Opin. Struct. Biol.* **7,** 528–532.
5. Retvield, A. & Simons, K. (1998) *Biochim. Biophys. Acta* **1376,** 467–479.
6. Gumbiner, B. & Louvard, D. (1985) *Trends Biochem. Sci.* **10,** 435–438.
7. Hadjiconstantinou, N. G. & Patera, A. T. (1997) *Int. J. Modern Phys.* **8,** 967–976.
8. Edidin, M. (1993) *J. Cell Sci. Suppl.* **7,** 165–169.
9. Zhang, F., Lee, G. M. & Jacobsen, K. (1993) *BioEssays* **15,** 579–588.
10. Allen, M. J., Lee, C., Pogany, G. C., Balooch, M., Siekhaus, W. J. & Balhorn, R. (1993) *Chromosoma* **102,** 623–630.
11. Allen, M. J., Bradbury, E. M. & Balhorn, R. (1995) *J. Struct. Biol.* **114,** 197–208.
12. Moy, V. T., Florin, E. L. & Gaub, H. E. (1994) *Colloids Surf.* **93,** 343–348.
13. Lee, G. U., Kidwell, D. A. & Colton, R. J. (1994) *Langmuir* **10,** 354–357.
14. Florin, E.-L., Moy, V. T. & Gaub, H. E. (1994) *Science* **264,** 415–417.
15. Boland, T. & Ratner, B. D. (1995) *Proc. Natl. Acad. Sci. USA* **92,** 5297–5301.
16. Hinterdorfer, P., Baumgartner, W., Gruber, H. J., Schlcher, K. & Schindler, H. (1996) *Proc. Natl. Acad. Sci. USA* **93,** 3477–3481.
17. Dammer, U., Hegner, M., Anselmetti, D., Wagner, P., Dreier, M., Huber, W. & Guntherodt, H.-J. (1996) *Biophys. J.* **70,** 2437–2441.
18. Allen, M. J. (1997) *IEEE Eng. Med. Biol.* March/April, 34–41.
19. Zhang, P.-C., Bai, C., Ho, P. K. H., Dai, Y. & Wu, Y.-S. (1997) *IEEE Eng. Med. Biol.* March/April, 42–46.
20. Ros, R., Schwesinger, F., Anselmetti, D., Kubon, M., Schafer, R., Pluckthun, A. & Tiefenauer, L. (1998) *Proc. Natl. Acad. Sci. USA* **95,** 7402–7405.
21. Wong, S. S., Joselevich, E., Woolley, A. T., Cheung, C. L. & Lieber, C. M., (1998) *Nature (London)* **391,** 52–55.
22. Willemsen, O. H., Snel, M. M. E., van der Werf, K. O., de Grooth, B. G., Greve, J., Hinterdorfer, P., Gruber, H. J., Schindler, H., van Kooyk, Y. & Figdor, C. G. (1998) *Biophys. J.* **75,** 2220–2228.
23. Fritz, J., Katopodis, A. G., Kolbinger, F. & Anselmetti, D. (1998) *Proc. Natl. Acad. Sci. USA* **95,** 12283–12228.
24. Frisbie, D., Rozsnyai, L. F., Noy, A., Wrighton, M. S. & Lieber, C. M. (1994) *Science* **265,** 2071–2074.
25. Moy, V. T., Jiao, J., Hillmann, T., Lehmann, H. & Sano, T. (1999) *Biophys. J.* **76,** 1632–1638.
26. Raab, A., Han, W., Badt, D., Smith-Gill, S. J., Lindsay, S. M., Schindler, H. & Hinterdorfer, P. (1999) *Nat. Biotechnol.* **17,** 902–905.
27. A-Hassan, E., Heintz, W. F., Antonik, M. D., D'Costa, N. P., Nageswaran, S., Schoenenberger, C.-A. & Hoh, J. H. (1998) *Biophys. J.* **74,** 1564–1578.
28. Hertz, H. (1882) *J. Reine Angew. Math.* **92,** 156–171.
29. Johnson, K. L., Kendall, K. & Roberts, A. D. (1971) *Proc. R. Soc. London Ser. A* **324,** 301–321.
30. Steigmann, D. J. (1999) *Arch. Rational Mech. Anal.* **150,** 127–152.
31. Helfrich, W. (1973) *Naturforschung* **28c,** 693–703.
32. Fung, Y. C. (1966) *Proc. Fed. Am. Soc. Exp. Biol.* **25,** 1761–1772.
33. Kleman, M. (1976*) Proc. R. Soc. London A* **347,** 387–404.
34. Rudd, R. E., McElfresh, M., Balsu, E., Balhorn, R., Allen, M. J. & Belak, J. in *Proc. Int. Conf. on Computational Nanoscience ICCN '02*, San Juan, PR, April 21–25, 2002, in press.
35. Evans, E. A. & Skalak, R. (1980) *Mech. Thermodyn. Biomembr.* (CRC, Boca Raton, FL).